



Polyacrylic acid-brushes tethered to graphene oxide membrane coating for scaling and biofouling mitigation on reverse osmosis membranes

Ali Ansari¹, Janire Peña-Bahamonde¹, Meng Wang, Devin L. Shaffer, Yandi Hu^{2, **}, Debora F. Rodrigues^{*}

Department of Civil and Environmental Engineering, University of Houston, Houston, TX-77004, USA



ARTICLE INFO

Keywords:

Reverse osmosis
Polyacrylic acid
Graphene oxide
Antiscalant
Antibiofouling

ABSTRACT

Reverse osmosis (RO) membranes are prone to fouling, which increases the cost of operation and decreases water recovery. In this study, a commercial membrane (ESPA2) was coated with an antiscalant material, *i.e.* polyacrylic acid (PAA), and an antimicrobial material, *i.e.* graphene oxide (GO), to reduce biofouling and scaling. Bare and modified membranes with polydopamine (ESPA2-PD), as a control, GO (ESPA2-GO), GO and PAA (ESPA2-GO-PAA), and PAA (ESPA2-PAA) were tested for their antiscalant and antibiofouling properties. ESPA2-GO and ESPA2-GO-PAA had the best performance. The latter showed ~15% and 10% increase in normalized water flux compared to ESPA2 in mineral scaling and biofouling tests, respectively. This improvement can be attributed to the decrease in surface charge and the increase in hydrophilicity of membrane surface by both GO and PAA coating. Moreover, the antimicrobial characteristic of GO played a crucial role in reducing biofouling and PAA slightly enhanced antiscalant property when coated on ESPA2 but it did not improve the antibiofouling property. These results highlight the importance of antimicrobial property of the coating for biofouling prevention and show antiscalant materials can be effective not only as an additive to the feed but also as a coating on the membrane to reduce scaling.

1. Introduction

Thin-film composite polyamide (TFC-PA) membrane is the standard industrial technology to be used in reverse osmosis (RO) systems for wastewater reuse or desalination of seawater and brackish water [1]. Improvements in TFC-PA membranes over the years have decreased the use of energy for seawater desalination to 3.4 kWh/m³ [2]. However, this number is still above the theoretical minimum value of 1.06 kWh/m³ for 50% recovery of seawater with 35,000 mg/L total dissolved solids (TDS) [2]. One of the main obstacles to make TFC-PA membranes more energy efficient is fouling, mainly caused by inorganic and biological materials known as scaling and biofouling, respectively [3,4]. Fouling reduces flux and increases the driving force needed for permeation; therefore, energy inputs are required for pre-treatment of the feed to prevent fouling or for cleaning the membrane to remove it.

One of the main sources of scaling on RO membranes, especially for

seawater desalination, is CaSO₄, which naturally occurs in the gypsum form (CaSO₄·2H₂O) at ambient temperature [5,6]. Preventing gypsum scaling is more challenging compared to other common salts like CaCO₃, since its crystallization is not pH-dependent [7]. As a result, changing pH does not prevent gypsum scaling. The most common method to mitigate gypsum scaling is by adding reagents called antiscalants or inhibitors to the feed water of a RO plant [8], which prevents gypsum scaling by either chelating with calcium ions or adsorbing on the gypsum nuclei [8–10]. Among the inhibitors, polyacrylic acid (PAA) has been reported to be more effective in preventing gypsum scaling [11]. However, a recent study has shown this antiscalant can be used as a food source by microbial communities naturally present in the seawater [12]. Biodegradation of antiscalants can have two negative effects on RO operation: 1) decreased inhibition effect on scaling and 2) increased biofouling due to an increase in bacteria growth. Therefore, it is important to utilize other approaches as well as design materials that can prevent scaling

* Corresponding author. Cullen College of Engineering Building 1, 4726 Calhoun Road, Room N107, Houston, TX, 77204, USA

** Corresponding author. Cullen College of Engineering Building 1, 4726 Calhoun Road, Room N117, Houston, TX, 77204, USA

E-mail addresses: yhu12@central.uh.edu, huyandi@pku.edu.cn (Y. Hu), dfrigirodrigues@uh.edu (D.F. Rodrigues).

¹ Equal contribution.

² Present Address: College of Environmental Sciences and Engineering, Peking University, Beijing 100871, China.

and biofouling.

Membrane surface modification is a widely researched technique to prevent scaling and biofouling. Among different materials used for surface modification, GO has shown great promise to prevent both scaling and biofouling. Our recent studies have shown that the addition of GO, not only improved antimicrobial properties of surfaces but also prevented biodegradation of polymers [13,14]. However, the effect of GO and a polymer coating on both scaling and biofouling has not been studied.

Recent studies have been conducted to coat membranes with nanocomposites to prevent both biofouling and mineral scaling. For instance, Tai et al. [15] synthesized a nanohybrid material with antimicrobial properties by *in situ* grafting PAA on graphene followed by attachment to silver nanoparticles. Another study by Wang et al. [16] showed that assembly of PAA and a potent antimicrobial agent, tobramycin, using the layer-by-layer technique led to a 26% decrease in bovine serum albumin and sodium alginate fouling and 99.6% bacterial inactivation.

Other studies functionalizing polyamide membranes with PAA demonstrated the application of such membranes in biomedical and environmental fields. These membranes presented antifouling activities, increasing water flux, and enhanced salt rejection [16–18]. In our recent study [5], GO coated membranes showed slightly better antiscalant properties compared to the polyamide membranes, unfortunately, the gypsum scale on GO coated membranes were harder to be removed during backwash. The addition of GO to the membranes have, however, added antibiofouling properties [19–23]. Therefore, it was hypothesized that the combination of GO and PAA could be used to enhance anti-fouling and antiscalant while maintaining membranes' transport properties. This hypothesis was initially investigated in the preliminary study by Ashfaq et al. [24]. In the Ashfaq et al. [24] study, modified polyamide membranes with an antimicrobial nanomaterial (GO) and an antiscalant polymer (PAA) showed good promise for these materials. However, their study, in some cases, did not investigate the performance of these membranes in realistic conditions simulating RO systems. For instance, the study was done with a single bacterial strain isolated from the Persian Gulf seawater in a rich medium (Luria Bertani), which precludes our understanding of such coatings in more realistic environmental conditions where diverse seawater microorganisms can have different behaviour in biofouling. Furthermore, no backwash was done on the fouled membranes to demonstrate how these coatings can affect the stability of the fouling layer. Although the study by Ashfaq et al. [24] has its own merits, their approach was not enough to elucidate the role of the PAA polymer on antiscalant and antibiofouling in more realistic conditions found in RO systems. In this present study, we made systematic improvements in the synthesis of the PAA-GO coating to maintain the membrane permeability similar to the non-coated membrane, and we also filled the knowledge gaps not addressed in the study by Ashfaq et al. [24] related to biofouling and scaling.

In this present study, a green synthesis approach was used to graft GO-PAA on membranes with no permeability reduction for the coated membranes, while investigating both antiscalant and antibiofouling properties in a RO system. The effect of coatings on scaling and biofouling were investigated in parallel with a lab-scale RO unit for the bare membrane ESPA2, ESPA2 coated with polydopamine (ESPA2-PD), ESPA2 coated with GO (ESPA2-GO), PAA (ESPA2-PAA), and GO & PAA (ESPA2-GO-PAA). A seawater microbial consortium enriched in synthetic seawater medium was used for the biofouling investigation to mimic real environmental conditions. The bare/coated membranes, before and after fouling and backwash experiments, were systematically characterized with various surface characterization techniques to understand physico-chemical interactions among aqueous species, microorganisms, and minerals.

2. Materials and methods

2.1. Materials

Graphite (<20 µm), sulfuric acid (H₂SO₄), dopamine hydrochloride, sodium nitrate (NaNO₃), ethylenediamine (ED), potassium permanganate (KMnO₄), H₂O₂ (30%), 10 mM Tris HCl buffer (>99%) BioXtra, osmium tetroxide (≥98%), and glutaraldehyde solution (25%) were purchased from Sigma Aldrich, Mo. CaCl₂.2H₂O and Na₂SO₄ were purchased from Fisher-Scientific, PA. SYTO9 and propidium iodide (PI) dyes were purchased from Invitrogen, USA. All chemicals used were ACS grade. Polyethylene frame was purchased from McMaster-Carr and the reverse osmosis membranes with polyamide active layer (ESPA2) were provided by Hydranautics Inc. (Oceanside, CA).

2.2. Synthesis of GO

A previously modified Hummer's method [25] was used to synthesize the graphene oxide nanosheets (GO). Briefly, concentrated H₂SO₄ (92 mL), NaNO₃ (2.0 g), and KMnO₄ (12.0 g) were added to 2.0 g of graphite for 16 h at 35 °C. Then, deionized water (DIW) (160 mL) was added to the previous solution, and the temperature was slowly increased to 90 °C. A mixture containing 400 mL of DIW and 40 mL of 30% H₂O₂ was added and stirred slowly after 30 min. Then, the mixture was washed several times by centrifugation (Thermo Scientific Sorvall Legend XTR Centrifuge) at 10,000 rpm for 10 min until supernatant pH 7. After which, the GO precipitate was sonicated in 2 L of DIW. After that, the GO dispersion was allowed to settle overnight, and the supernatant was removed. Finally, the wet powder was dried in a freeze drier (Labconco, Freezone 4.5 L, -84 °C benchtop freeze dryer) for future use.

2.3. Membrane coating

2.3.1. ESPA2 coating with graphene oxide

Polyamide membranes were functionalized with graphene oxide following the method described by Zhang et al. [26]. Briefly, the membranes were cleaned with DIW following isopropanol prior to the experiment. Then, the ESPA2 polyamide membranes were clamped between a polyethylene frame and an aluminum sheet to isolate the polyamide active layer of the membrane. The membrane surface was exposed to a solution at pH = 7.0 containing 2 mg/mL of dopamine hydrochloride in 10 mM Tris buffer for 1 h to allow self-polymerization of dopamine on top of the polyamide active layer, forming an adhesive layer on top of the membrane. After that, the membranes were rinsed several times with DIW to remove the unreacted monomer. Then, the membrane was coated with GO via ethylenediamine as a cross-linking reagent. Briefly, 1% (w/w) ethylenediamine was mixed with an aqueous solution containing 1 mg/mL of GO during 1 h. After that, the solution was poured on the membrane and shaken for 2 h. Then, the unreacted GO was removed washing the membrane (ESPA2-GO) with DIW several times.

2.3.2. ESPA2 and ESPA2-GO functionalization with polyacrylic acid

A grafting from method was used to attach the polyacrylic acid polymer (PAA) to the surface of the membrane. ESPA2-GO was functionalized with PAA polymer brushes to obtain ESPA2-GO-PAA via a surface-initiated polymerization, since it is well-known that the GO can act as an initiator and producing polymerization on top of its structure [27–30]. Similarly, ESPA2-PAA was functionalized as a control membrane with acrylic acid (AA) monomer using a previously described method [18,31]. Both procedures were similar. Briefly, the membranes were clamped in a frame to expose only the active layer. Then, an aqueous solution containing AA (20% (w/w)) was poured on the membrane and irradiated under a UV lamp (Spectroline, Model EA-160 at long wave ultraviolet 365 nm) for 1 h to allow self-polymerization on top of the membrane. After that, the solution was poured off the

membranes (ESPA2-GO-PAA and SPA2-PAA) and the membranes were washed several times with DIW to remove unreacted monomers and homopolymers.

2.4. Physico-chemical characterization of coatings on membranes

The functional groups on top of the surface of the membrane were evaluated by Attenuated total reflection Fourier-transform infrared spectroscopy (ATR-FTIR). The spectra were obtained with a nominal spectral resolution of 4 cm^{-1} in transmittance mode from 4000 to 600 (cm^{-1}) wavenumbers using a HgCdTe detector equipped with a Digilab FTS 7000. To further investigate the stability of the coatings on the membranes, Raman spectroscopy was collected before and after using the membranes in the RO system. Raman spectroscopy was done using HORIBA iHR320 Spectrometer equipped with a Synapse CCD with a laser at 532 nm.

The GO and the surface of the bare and coated membranes were analyzed using Scanning electron microscopy (SEM) at various magnifications. The Nova NanoSEM 230 was used. The accelerating voltage was 10 kV. Before analysis, gold coating on samples was done for 30 s (Denton Desk V).

The elemental composition and chemical structure of the different functional groups attached to the surface membrane was evaluated by analyzing the X-ray photoelectron spectroscopy (XPS) spectra with a PHI Quantera SXM Scanning X-ray Microprobe and an excitation source of Al K α (1486.6 eV). The binding energy was calibrated at 284.8 eV (C–C bonds). High-resolution spectra were acquired. The pass energy, energy step size, and time step were 23.5 eV, 0.2 eV, and 50 ms, respectively. For fouled membrane surfaces, scalant crystal structures were analyzed by X-ray diffraction (XRD) using Rigaku MiniFlex 600 diffractometer with a Cu anode (40 kV and 15 mA). XRD pattern was also acquired for membranes before filtration in RO. Biofilms were characterized by confocal laser scanning microscopy (CLSM) using the Leica DM 2500 Microscope. Measurements were determined under a 10x objective at 0.30 numerical aperture. COMSTAT software was used for biomass and average thickness calculations.

Dynamic light scattering (DLS) was used to measure the Surface ζ -potential of the membranes in a Zetasizer Nano, Malvern Industry Ltd instrument. The membranes were analyzed in the ζ -potential cell between the two electrodes. A standard solution at pH 9 of polystyrene latex particles (DTS1235, Malvern Instruments) was used as a tracer. After that, the electrophoretic mobility of the tracer was determined at different distances from the membrane, i.e., 125, 250, 500, 750, and 3000 μm , to calculate the surface ζ -potential of the membrane.

The surface hydrophilicity of the bare and coated membranes was determined by the sessile drop method. Membranes were dried overnight before the test. The images of water drops were analyzed with ImageJ to measure the contact angle between the drop and the surface.

Atomic force microscopy measurements (AFM, Veeco Instrument) were employed for surface topography characterization of bare and coated membranes. Before the measurements, membranes were dried and cut into $1\text{ cm} \times 1\text{ cm}$ pieces and adhered to a carbon disk with epoxy resins. In order to minimize the forces between the AFM tip and the surface, tapping mode was used. The surface roughness was measured in triplicate on sections of $10\text{ }\mu\text{m} \times 10\text{ }\mu\text{m}$ with the Nano-scope Analysis 1.5 software.

2.5. Membrane performance characterization

2.5.1. Permeability and salt rejection

A bench-scale 3-cell crossflow RO filtration unit (Fig. S2) with a 24.2 cm^2 active area and no spacer was used to measure permeability and selectivity of the membranes. The membranes were compacted with DIW at 200 psi and 400 psi for permeability and salt rejection tests, respectively, until the permeate flux became stable. Permeate flux was measured at 200 psi and salt rejection at 400 psi transmembrane

pressure. For both tests, crossflow velocity was 21.4 cm/s and the feed solution temperature were maintained at $25 \pm 0.5\text{ }^\circ\text{C}$ using a recirculating chiller. To calculate the permeate flux (J_w) the volume of pure water was divided by the membranes' active area and time. To evaluate the salt rejection, filtering of a 50 mM solution of NaCl was done. By using Equation (1), salt rejection (R) was calculated after measuring the salt concentration in the feed (C_f) and permeate (C_p) by a conductivity meter (VWR symphony B40PCID)

$$R = \left(\frac{C_f - C_p}{C_f} \right) \times 100 \quad (1)$$

2.6. Gypsum scaling experiments

Calcium sulfate solutions were prepared from sodium sulfate anhydrous and calcium chloride dihydrate solutions. The mixed $\text{CaCl}_2 \cdot 2\text{H}_2\text{O}$ and Na_2SO_4 solution compositions, pH, and ionic strength were calculated. The saturation indices, with respect to gypsum ($\text{CaSO}_4 \cdot 2\text{H}_2\text{O}$) and basanite ($\text{CaSO}_4 \cdot 0.5\text{H}_2\text{O}$) at $25\text{ }^\circ\text{C}$ (Table S1), were calculated with Geochemist's Workbench (GWB, 11.0. 6, Aqueous Solution LLC). Mineral scaling on the reverse osmosis membrane occurred in two ways: direct heterogeneous crystallization on the membrane and homogeneous precipitation in solution with later deposition on the membrane. In Table S1, the bulk solution was under-saturated with respect to gypsum ($\text{SI} = -0.13$). Because of the concentration polarization, the saturation index for gypsum shown in Table S1 at the membrane surface exceeded the one in the bulk solution ($\text{SI} = 0.02$). That caused heterogeneous precipitation of gypsum on the surface of the membranes.

Mineral scaling experiments were conducted using a bench-scale crossflow reverse osmosis system, different from the system that was used in permeability, salt rejection, and biofouling tests. The experimental setup consisted of two tanks: one tank was filled with DIW for stabilization and backwashing, and the other tank was filled with a well-mixed solution for membrane conditioning/scaling. The feed solution was pumped to the RO system. The crossflow rate was 15.8 cm/s compared to 21.4 cm/s for permeability, salt rejection, and biofouling tests. The schematic of the system has been presented in our previous work [5]. The trans-membrane pressure of the reverse osmosis system was maintained at 500 psi vs. 200 psi for permeability and biofouling and 400 psi for salt rejection. Each run was carried out with the same crossflow velocity, temperature, and pressure to ensure a common basis for the comparison of all scaling tests. No spacer was used in the RO cell.

The protocols of membrane scaling tests involved three processes: DIW stabilization, mineral scaling, and backwash. The stabilization of the membranes was done at 500 psi. After stabilization the scaling process was carried out for 6 h. During the whole scaling process, the volume of permeate was collected and measured with the increment of the time. Finally, membrane backwash was performed immediately after the scaling experiments with DIW at the same crossflow rate and pressure until the permeate flux was stable. To calculate the normalized flux, initial flux of the scaling experiments was used for the scaled membranes; while to calculate the recovered flux, the DIW flux was used for normalization. The washed membranes were analyzed with XRD to identify any remaining precipitates. Another set of experiments was done to characterize mineral scales on the membrane after scaling without backwash. At the end of the scaling experiments, mineral phase as well as the morphology of the precipitates were characterized using XRD and SEM.

2.6.1. Biofouling experiments

Before and after each test, the bench-scale 3-cell crossflow RO filtration unit was washed three times with DIW, followed by circulation of 70% ethanol to disinfect the system. To clean the ethanol from the system, three more washings with DIW was done. The biofouling test was done by filtration of a marine consortium through the membranes. Sampling, enrichment, and consortium composition have been

presented in our previous study [32]. Before filtration, membranes were irradiated for 15 min with UV to remove any microorganisms attached to them [33,34]. Then the membranes were mounted in RO cells without spacer. After stabilization of the membranes as described before, 200 mL of synthetic seawater (Table S2) was added to 8.8 L of DIW while stirring at 200 rpm. After the membrane was equilibrated with the salts (2–3 h), 60 mL of the marine consortium at late exponential phase, which was washed three times with 0.85% NaCl and suspended in an OD equal to 0.65, was added to the feed solution to achieve initial cell concentration of 10^7 CFU/mL. Cells were filtered through the membranes for 45 min to allow them to attach to the membrane surface, after that, 9 mL of nutrient broth (NB) (Table S2) was added to the feed. The final concentration of NB in the feed was 0.1%. The temperature of the feed was kept at 25 ± 0.5 °C, trans-membrane pressure was 200 psi, and crossflow velocity was 21.4 cm/s. Filtration was continued for 48 h. By dividing the permeate flux every 6 h by initial permeate flux, the normalized flux was calculated.

After the test was done, six coupons of the membranes were cut. CLSM analysis of the biofilm was done on three coupons following Nguyen *et al.* protocol [21]. The other three coupons were analyzed via SEM. For the SEM images, the bacterial cells on the three other coupons were fixed by 2% glutaraldehyde solution and osmium tetroxide [21]. After filtration, the cleaning of the membranes was done with DIW at the same crossflow velocity and pressure, until permeate flux became stable.

3. Results and discussion

3.1. Synthesis and characterization of coated membranes

SEM images of GO at different magnifications can be found in Figs. S1 and a complete characterization of GO is presented in our previous work [35]. In this work, we modified a commercial reverse osmosis polyamide membrane (ESPA2) with polydopamine (ESPA2-PD), graphene oxide (ESPA2-GO), polyacrylic acid (ESPA2-PAA), and polyacrylic acid as a polymer brush on top of the surface of graphene oxide (ESPA2-GO-PAA). The binding mechanisms between GO and PAA can be due to the surface-initiated polymerization properties that GO exhibited since it has been proved that UV-light can promote the GO activation and produce the photopolymerization of vinyl polymer brushes [27,30,36,37]. The coated membranes were well characterized by different techniques.

Fig. 1 shows the comparison of the ATR-FTIR spectra of the ESPA2, ESPA2-PD, ESPA2-GO, ESPA2-GO-PAA, and ESPA2-PAA membranes in the range between 4000 and 650 cm^{-1} . The polyamide membrane presented the following peaks at 1663, 1541 cm^{-1} , and 1609 cm^{-1} , respectively, C=O stretching, N-H bending and the C=C stretching. When the membrane was functionalized with GO, little differences were observed in the spectra, since both materials had similar functional groups. Furthermore, the ATR-FTIR spectra of the ESPA2-GO membranes, showed a new peak at ~ 1720 cm^{-1} corresponding to the stretching of the carbonyl (C=O) group, which are present in carboxyl acid, anhydrides, and ester groups. This peak is absent in the ESPA2 and ESPA2-PD membranes [38]. The functionalization with PAA on top of graphene oxide was further demonstrated by the intensity of the carbonyl (C=O) band, due to the contribution of carboxylic acid groups present in the polymer [39]. Furthermore, the spectrum showed a new peak around 2950 cm^{-1} , compared to ESPA2, which was attributed to the C-H stretching from both, PAA and GO functionalization [31].

The addition of GO and PAA to the bare membrane, could potentially enhance the hydrophilicity of the membrane due to the presence of more hydroxyl groups. The hydrophilicity was confirmed by the water contact angle measurements (Table 1). ESPA2-PD and ESPA2-GO membrane exhibited the lowest water contact angles measured among all tested membranes due to the presence of the amine groups for the former and the carboxyl and hydroxyl groups for the latter [40–44]. Modification of the bare membrane with PAA, increased the hydrophilicity of the

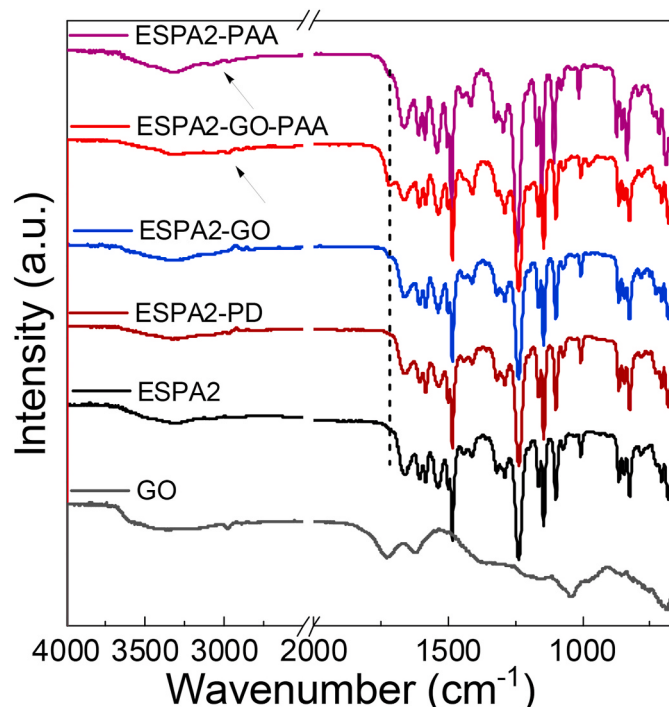


Fig. 1. ATR-FTIR spectra of GO, bare, and coated membranes.

membrane [31,45]. However, no significant differences were observed compared to ESPA2-GO when AA was grown on top of the membrane.

The surface properties of the membrane were further investigated by the analysis of the ζ -potential measurements. Table 1 shows that the addition of GO and PAA induced a more negative surface charge, which correlated well with the decrease in contact angles. This decrease in the ζ -potential is due to the presence of more carboxyl groups from the GO and PAA, their deprotonation generated a more negative surface charge [46,47]. Meanwhile, protonation of amine groups on ESPA2-PD made the surface less negatively charged [44].

Raman spectra further demonstrate the modification of the coated membranes. Fig. S3 showed the characteristic peaks corresponding to the symmetric C–O–C stretching and the phenyl ring vibration of the polyamide membranes at 1147 cm^{-1} and 1585 cm^{-1} , respectively [48–50]. It is well known, that GO has two characteristic broad peaks, D and G band, at 1350 cm^{-1} and at 1590 cm^{-1} , respectively [51]. The modification of ESPA2 with GO (ESPA2-GO membrane) resulted a broader peak at 1585 cm^{-1} due to the combined contributions from the phenyl ring vibration and the G band of GO. Furthermore, its incorporation also induced changes in the ratio (I_{1147}/I_{1585}) between the C–O–C stretching and the phenyl ring vibration band [43,50]. Table 1 shows the calculation of the ratio for all the coated membranes. The (I_{1147}/I_{1585}) ratio significantly decreased from 1.6 to 1.2 when we introduced GO in the bare membrane, this decrease confirmed the introduction of graphene oxide to the ESPA2 membrane. Furthermore, the polymerization with AA also showed a slight decrease on the I_{1147}/I_{1585} ratio. Moreover, the polymerization on top of the membrane was further demonstrated by XPS, SEM, and AFM.

XPS provided information about the atomic percentages of chemical elements found in the membranes. The elemental composition of the coated membranes is shown in Table 1. The main elements present on the surfaces were carbon (C), nitrogen (N), oxygen (O), aside for the presence of sulfur (S) shown only in the commercial membrane (ESPA2) that was due to the presence of a thin layer of polysulfone on the back of the commercial bare membrane (ESPA2). Moreover, the energy peaks from C, O and N exhibited different ratios compared to the bare membrane, which confirmed that the bare membranes were successfully

Table 1

Elemental composition, Raman intensity ratio, water contact angle, surface ζ -potential, permeability, and salt rejection properties of bare and coated membranes.

Sample	XPS			Raman (I_{11145}/I_{1581})	Surface ζ -potential (mV)	Water contact angle (°)	Permeability (L/m ² .h.bar)	Salt rejection (%)
	C (%)	N (%)	O (%)					
ESPA2	76.3	13.4	9.8	1.6	-28 ± 2	32 ± 2	5.1 ± 0.2	98.6 ± 0.1
ESPA2-PD	74.5	8.7	16.8	1.5	-22 ± 1	20 ± 1	5.2 ± 0.2	97.2 ± 0.1
ESPA2-GO	71.0	7.3	21.7	1.2	-35 ± 2	22 ± 2	5.2 ± 0.3	97.4 ± 0.1
ESPA2-GO-PAA	67.7	7.5	24.8	1.1	-38 ± 4	21 ± 2	5.3 ± 0.2	96.7 ± 0.3
ESPA2-PAA	70.3	11.0	18.7	1.7	-34 ± 2	28 ± 1	5.4 ± 0.1	97.4 ± 0.1

modified with GO and PAA [38,43]. The atomic percentage of oxygen (1s, 530 eV) on the surfaces of ESPA2-GO membranes increased compared to the bare membranes, while the atomic percentage of nitrogen (1s, 400 eV) decreased. The functionalization of the bare membrane with polydopamine produced a decrease in the nitrogen contribution compared to the bare membrane. This decrease could be attributed to the low amount of nitrogen on the structure of the polydopamine and the coating with a thin layer of polydopamine. However, when GO got attached to the surface of ESPA2-PD, the contribution of nitrogen was almost similar, while the contribution of oxygen slightly increased due to the contribution of the functional groups of GO, such as COOH, C=O, and -OH.

The polymerization of AA further increased the atomic composition of oxygen due to the large amount of carboxylic acid in the structure of the polymer. The analysis of the area ratio of O 1s/N 1s for the bare membrane ($r = 0.7$) relatively increased to 2.0 and 1.6 for the ESPA2-GO and ESPA2-PAA, respectively, indicating that GO and PAA were grafted on top of the bare membrane [52]. These results suggested that GO and PAA adhered to the surface of the bare membrane.

By SEM and AFM, we evaluated the surface morphology and surface roughness of the bare and coated membranes as shown in Figs. 2 and S4. SEM analysis showed the overall surface morphology of the membranes. The SEM images suggested that the incorporation of GO on the bare membrane (ESPA2) changed the overall aspect of the surface indicating the successful incorporation of the GO on the surface of the bare membrane (Figs. 2c and S4). By the AFM analysis, the membrane functionalization with GO (Fig. 2c), to form ESPA2-GO membrane, showed that the membrane surface roughness ($R_q = 67.83 \pm 8.96$ nm) did not significantly change in comparison with the bare membrane ($R_q = 69.17 \pm 1.62$ nm) ($p = 0.8114$) and was higher than the respective control, polydopamine coated membrane (ESPA2-PD) (55.30 ± 10.36) ($p = 0.0838$) (Fig. 2b). The fact that the introduction of GO (ESPA2-GO) increased the membrane surface roughness compared to ESPA2-PD indicates that there could be some aggregation of GO on top of the membrane surface [42].

When the PAA polymer brush was introduced to the surface of the GO modified membrane, the surface roughness of the PAA functionalized GO coated membrane ($R_q = 70.4 \pm 2.4$ nm) ($p = 0.6524$) did not significantly change compared to the pristine GO coated membrane.

However, the modification with PAA only with bare membrane to form ESPA2-PAA membrane showed a significant decrease in the surface roughness, ($R_q = 62.7 \pm 1.4$ nm, $p = 0.0063$), which was consistent with the morphology observed by SEM. We could observe a denser and compressed layer produced by the polymerization of PAA on top of the polyamide membrane [18,39]. This may be related to the molecular weight and conformation of the PAA polymer brush grafted on the membrane surface [18]. Besides, comparing the surface roughness of bare and modified membranes, we observed that the surface roughness values varied but were comparable in terms of magnitude, indicating that the current synthesis method was successful for graphene oxide and polyacrylic acid modification.

3.2. Permeability and salt rejection

The permeability of bare and coated membranes is presented in

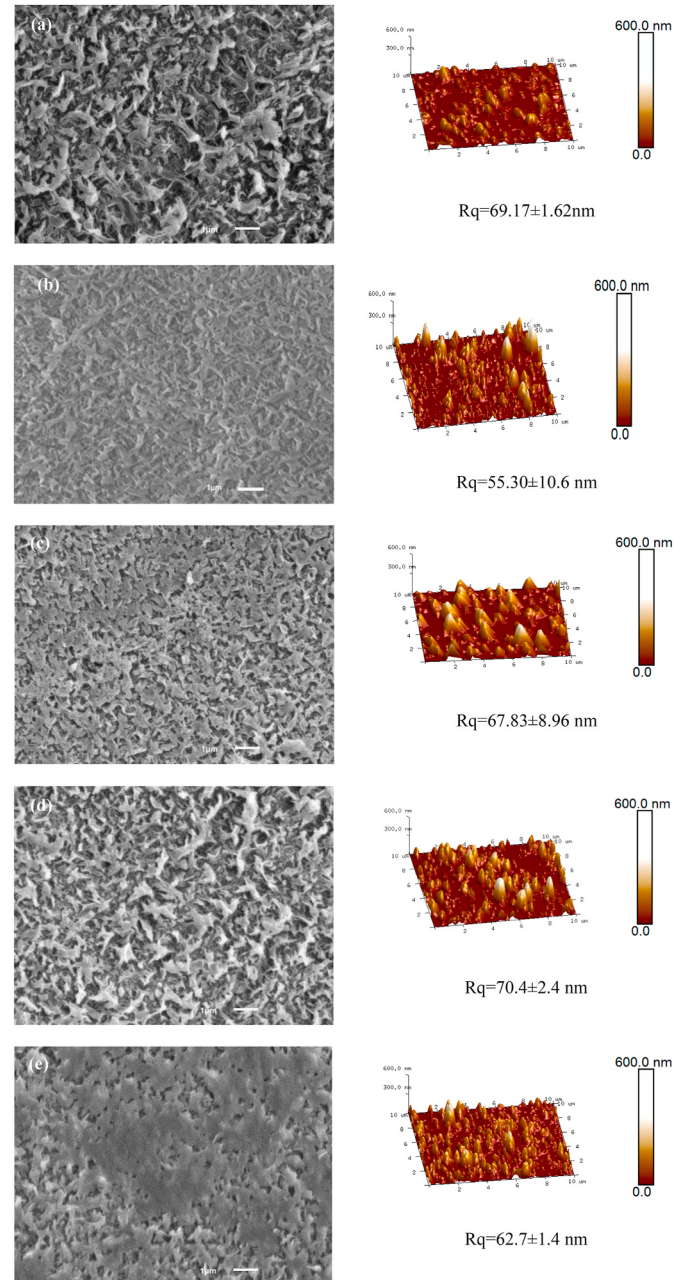


Fig. 2. SEM images at 10,000 \times magnification and AFM images with scale bar: 10 μ m, for (a) ESPA2, (b) ESPA2-PD, (c) ESPA2-GO, (d) ESPA2-GO-PAA, and (e) ESPA2-PAA.

Table 1. The water permeability did not change significantly after coating the ESPA2 with, PD, GO and PAA, however, the average water permeability was slightly higher for the coated membranes compared to the bare membranes. In terms of salt rejection, all the coated membranes

showed a slight decrease compared to the bare membrane. The salt rejection was 98.6 ± 0.1 , 97.2 ± 0.1 , 97.4 ± 0.1 , 96.7 ± 0.3 , and 97.4 ± 0.1 for ESPA2, ESPA2-PD, ESPA2-GO, ESPA2-GO-PAA, and ESPA2-PAA, respectively. ESPA2-PD, ESPA2-GO, and ESPA2-PAA did not show a statistically significant difference from each other. However, ESPA2-GO and ESPA2-GO-PAA were different ($p = 0.0085$) as well as ESPA2-GO-PAA and ESPA2-PAA ($p = 0.0154$) and ESPA2-PD and ESPA2-GO-PAA ($p = 0.0339$). The water permeability results showed that the coating materials generated a thin layer on the membrane and did not add resistance to the mass transfer across the membrane [53]. Moreover, the coating materials *i.e.* GO and PAA, made the surface more hydrophilic by introducing hydroxyl and carboxyl functional groups, therefore the water flow through the membrane was facilitated and the water permeability increased [16]. The increase in water permeability, while the salt rejection decreased, could be attributed to the possible penetration of polydopamine into the PA layer. This ingress of the polydopamine could have weaken the hydrogen bonds in the PA layer, therefore, increased the mobility of the PA chains and altered the water and salt passage through the PA layer [54,55].

3.3. Gypsum scaling experiments

As shown in Figs. 3 and S5a, the flux decay rate of GO modified membranes was slower than the bare membranes. This observation indicates that GO coatings can retard scaling on the membrane surfaces in contrast to ESPA2 membranes, which is in line with our previous study [5]. Furthermore, when the PAA polymer brush was introduced on the surface of GO modified membranes, the flux decay rate of GO-PAA coated membranes was almost the same as only GO and only PAA modified membranes. In addition, the flux decay rate of ESPA2-PD was smaller than the ESPA2 and ESPA2-PAA coated membranes but presented similar flux decay rates to ESPA2-GO and ESPA2-GO-PAA membranes. Therefore, all the coated membranes have shown better antiscalant properties compared to the bare membrane.

To check the mineral structure of crystals on ESPA2, ESPA2-PD, ESPA2-PAA, ESPA2-GO, and ESPA2-GO-PAA membranes, XRD measurements were conducted. As shown in Fig. S6b, the mineral precipitates on all the above-mentioned membranes were gypsum. No other forms of the mineral were detected. Therefore, mineral phase of CaSO_4 was not affected by the coatings on the bare membrane.

The improvement in scaling resistance by different coatings could be attributed to the changes in surface hydrophilicity. Based on the classical nucleation theory, the higher the membrane hydrophilicity, confirmed by decreased water contact angles (Table 1), the lower the liquid-substrate interfacial energy, which increases the nucleation energy barrier on the hydrophilic membranes modified with PD, GO, PAA, and GO-PAA coatings [4]. Similarly, Jaramillo et al. [56] observed a slower flux decline of zwitterion-modified membranes compared to the control RO membrane during gypsum scaling. In this study, they revealed that the decreased interfacial energy between the membrane and water were due to a higher surface hydrophilicity of zwitterion coatings, which made gypsum nucleation on membranes unfavorable. It should be noted that the higher surface hydrophilicity of PD coated membranes led to a better anti-scaling property than ESPA2 and ESPA2-PAA membranes. The similar flux decay rates among ESPA2-PD, ESPA2-GO, and ESPA2-GO-PAA membranes were due to alike surface hydrophilicities, as indicated by the contact angle results.

DIW was used to clean the membranes since it is a common practice to remove fouling [2,5,55,57]. After membrane backwash, as shown in Fig. 3, the normalized permeate flux recovery rates of the ESPA2, ESPA2-PD, ESPA2-GO, ESPA2-GO-PAA, and ESPA2-PAA were 0.89, 0.91, 0.85, 0.65, and 0.80, respectively. Raman spectra (Fig. S7) and I_{1145}/I_{1581} ratio (Table S3) of backwashed membranes showed similar results compared to membranes before the scaling test, which proved the stability of the coatings during the scaling tests and backwash.

The relatively low permeate flux recovery rates ($\leq 85\%$), except for

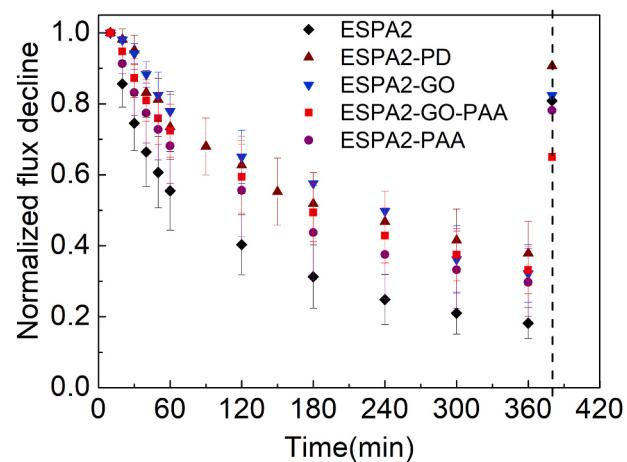


Fig. 3. Gypsum scaling and backwashing behavior of ESPA2, ESPA2-PD, ESPA2-GO, ESPA2-GO-PAA, and ESPA2-PAA at 500 psi, 15.8 cm/s crossflow rate, and 25 °C. Note: the initial fluxes in the scaling experiments were used to normalize the scaling fluxes, and DIW flux was used to normalize the recovered flux. The last data point shows the permeate flux after backwashing with DIW. Standard deviations are represented as the error bars.

bare and PD coated membranes, indicated that some gypsum scalants were strongly attached to the GO and/or PAA modified membrane surfaces and could not be detached during backwash. Mi et al. [58] also described that gypsum precipitates on polyamide membranes were harder to clean compared to those on cellulose acetate (CA) membranes. This phenomenon was attributed to the interactions between calcium ions and the functional groups of different membranes. In the case of polyamide membranes, the carboxylic functional groups could form complexes with calcium ions, while the hydroxyl functional groups found in CA membranes could not. Furthermore, in our prior study, the carboxyl functional groups of GO modified membranes could form strong chemical bonds with calcium ions, therefore making surface-induced precipitates harder to be removed [5]. In this present study, when the mixture of GO and PAA coatings were grafted on the bare membranes, the amount of carboxyl groups on ESPA2-GO-PAA membranes further increased compared to ESPA2-GO and ESPA2-PAA membranes. The carboxyl groups led to a more negative surface charge of GO-PAA coatings compared to the other coatings (Table 1) because more carboxyl groups tend to deprotonate on GO-PAA coated membrane surfaces. Therefore, with the presence of more carboxyl groups on the membrane surface, the chemical bonding between these coatings and gypsum precipitates became stronger, which led to a low flux recovery rate of the ESPA2-GO-PAA membranes. For the PD coated membranes, the highest flux recovery rate was due to the low density of carboxyl functional groups on the membrane surface able to bind to calcium ions, as indicated by its less negative charge compared to the other four membrane surfaces (Table 1). Hence, membranes with less negative surface charge indicates reduced amounts of carboxyl functional groups as well as weaker interactions between gypsum precipitates and the membrane surfaces, and thus, higher flux recovery rate during membrane backwash.

The flux recovery rates were consistent with XRD measurements of the membranes after backwash. As shown in Fig. S6c, the characteristic peaks for gypsum at $2\theta = 11.58$ were identified for all membranes except for ESPA2-PD membranes, indicating that some gypsum crystals remained on the membrane surfaces after the backwash experiments (Fig. S6c). The ESPA2-PD membrane, however, had the highest recovered flux due to the easy removal of gypsum crystals. Therefore, almost no peaks belonging to gypsum were shown on the XRD pattern for ESPA2-PD.

To determine the mineral morphology of the gypsum scaling on the bare and coated membranes; SEM analysis was performed as shown in

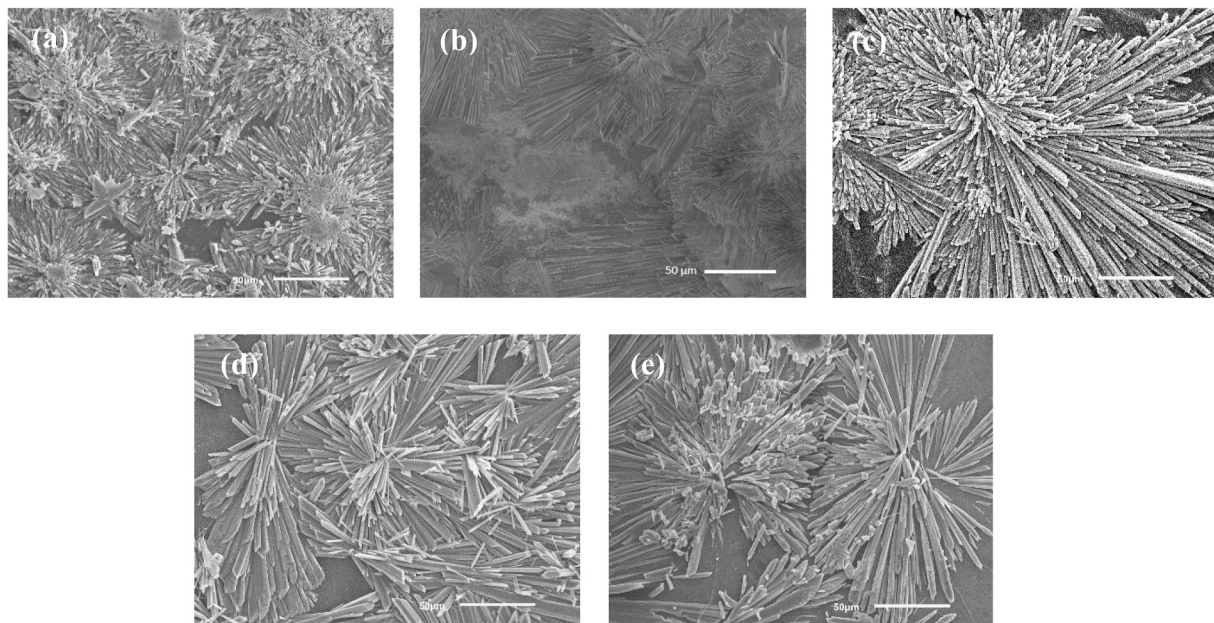


Fig. 4. SEM images of gypsum scaling on (a) ESPA2 membrane surface, (b) ESPA2-PD membrane surface, (c) ESPA2-GO membrane surface (d) ESPA2-GO-PAA membrane surface, and (e) ESPA2-PAA membrane surface. Note the scale bar is 50 μm for all images (500 \times magnification).

Fig. 4. A rosette-shaped flower formed on all the membranes' surfaces. The coverage of gypsum crystals on the ESPA2 membrane surface (Fig. 4a) was greater than that of the ESPA2-GO membrane surface (Fig. 4c), which correlates with the higher flux decline observed for these membranes in the scaling experiment. The inhibited flux decay rate of PD coated membranes compared to ESPA2 was consistent with the SEM images showing less coverage of gypsum precipitates on ESPA2-PD membrane surfaces (Fig. 4b). Besides, the precipitated gypsum layer on the ESPA2-GO-PAA membrane surface (Fig. 4d) became less dense in contrast to the ESPA2 (Fig. 4a) leading to the inhibition of permeability decay.

3.4. Biofouling experiments

The normalized and non-normalized permeate flux decline over time are shown in Fig. 5 and Fig. S5b for ESPA2, ESPA2-PD, ESPA2-GO,

ESPA2-GO-PAA, and ESPA2-PAA, respectively. The initial permeate fluxes of the membranes after the addition of the medium and bacteria were almost the same (Table S4). For the first 24 h, the normalized permeate flux changes were similar for all the membranes, however, at 30 h the ESPA2-GO started to show higher normalized permeate flux compared to the other membranes. As filtration continued up to 48 h, the ESPA2-GO and ESPA2-GO-PAA showed higher permeate flux, indicating less biofouling compared to ESPA2, ESPA2-PD, and ESPA2-PAA. Washing the membranes at the end of the biofouling test with DIW water showed that the biofilm on ESPA2-GO and ESPA2-GO-PAA was easier to clean, as the normalized permeate flux increased to 0.97 ± 0.01 and 0.90 ± 0.03 for the two membranes, respectively. While permeate flux increased to 0.85 ± 0.01 for ESPA2, 0.85 ± 0.01 for ESPA2-PD, and 0.84 ± 0.02 for ESPA2-PAA.

The biofilm layer that accumulated on the fouled membranes was analyzed with CLSM (Fig. 6) and SEM (Fig. 7). The biomass and average thickness were significantly lower for ESPA2-GO and ESPA2-GO-PAA compared to ESPA2 and ESPA2-PAA, which confirms the filtration test results. For ESPA2-PD, biomass was significantly lower than the bare

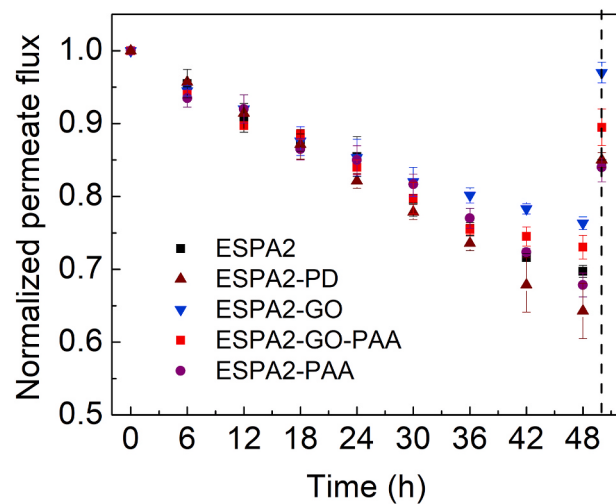


Fig. 5. Biofouling and backwashing behavior of ESPA2, ESPA2-PD, ESPA2-GO, ESPA2-GO-PAA, and ESPA2-PAA at 200 psi, 21.3 cm/s crossflow rate at $25 \pm 0.5^\circ\text{C}$. The last data point shows the permeate flux after backwashing with DIW. Standard deviations are represented as the error bars.

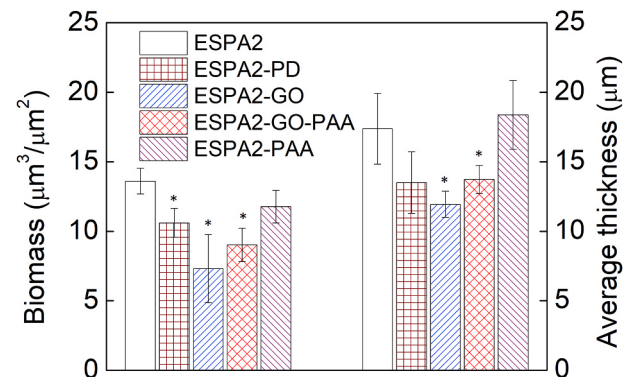


Fig. 6. CLSM results for bare and coated membranes for biofouling by seawater consortium at 200 psi, 21.3 cm/s crossflow velocity, and $25 \pm 0.5^\circ\text{C}$. The * shows a statistically significant difference in biomass and average thickness compared to the bare membrane with a 95% confidence interval. The standard deviations are represented in the graph as error bars.

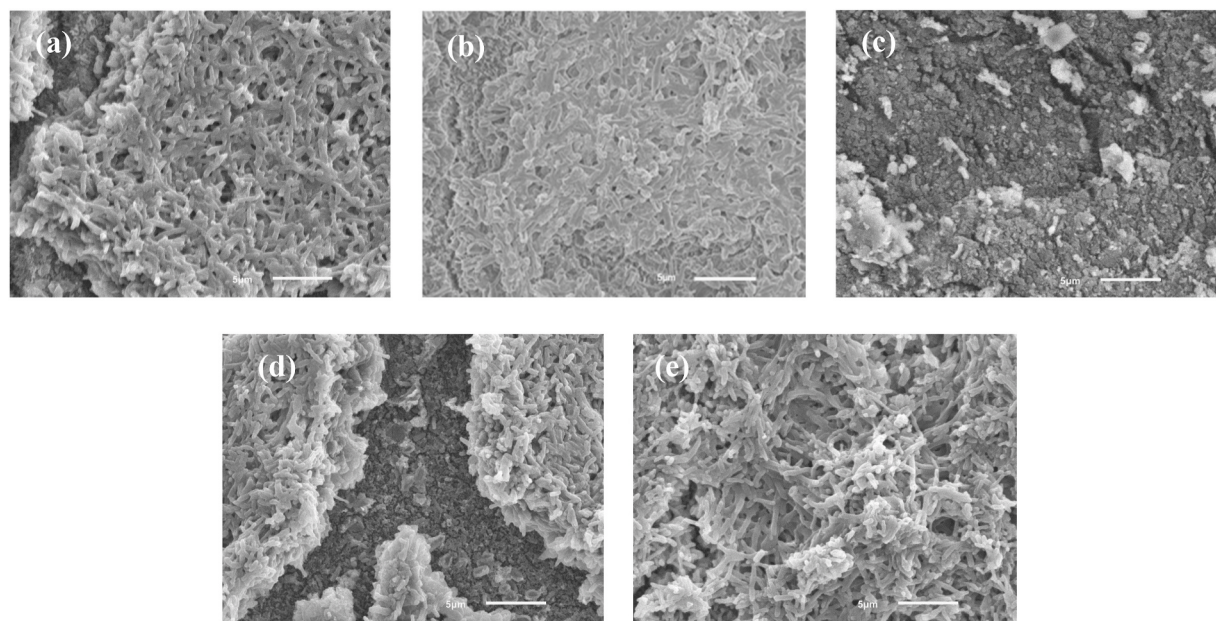


Fig. 7. SEM images for the different membrane surfaces: (a) bare surface, (b) PD modified, (c) GO modified, (d) GO-PAA modified, and (e) PAA modified after biofouling test by a seawater consortium at 200 psi, 21.3 cm/s cross-flow velocity at $25 \pm 0.5^\circ\text{C}$. Note the scale bar is 5 μm for all images (4000 \times magnification).

membrane, but the average thickness was not. SEM images showed that the biofilm covered almost all the ESPA2, ESPA2-PD, and ESPA2-PAA surfaces, while on ESPA2-GO and ESPA2-GO-PAA some parts were not covered with biofilm with some dead bacteria identifiable on those parts. The biofilm layer on ESPA2-PD looks denser compared to the bare membrane, that might be the reason why same flux decline was obtained for PD coated and bare membrane, although the biomass volume was smaller for PD coated compared to bare membrane.

The antibiofouling characteristics of the ESPA2-GO and ESPA2-GO-PAA can be attributed to the antimicrobial properties of GO and enhancement in the physical properties of these membranes compared to ESPA, ESPA2-PD, and ESPA2-PAA. Generally, a hydrophilic material decreases biofouling by forming a water layer on the membrane surface, which prevents the adhesion of bacteria and organic molecules on the surface [16]. Furthermore, a rough surface is more prone to entrapment of foulant on the surface by foulant-membrane interactions [1]. As a result, a smoother and more hydrophilic surface is expected to show better antibiofouling properties. In terms of surface charge, it is expected that a more negatively charged surface will repel negatively charged bacteria and organic molecules, hence increasing antifouling properties.

As discussed before, the ESPA2-GO and ESPA2-GO-PAA were more hydrophilic compared to the two ESPA2 and ESPA2-PAA and had more negative surface charges compared to the bare ESPA2 and ESPA2-PD membranes. These features can potentially contribute to the less biofouling observed on ESPA2-GO and ESPA2-GO-PAA compared to ESPA2, ESPA2-PD, and ESPA2-PAA. PD coating increased hydrophilicity which is beneficial for biofouling resistance, however, since the surface became less negatively charged with PD coating, changes in the surface charge acted against the biofouling resistance, therefore, same flux decline was observed for PD coating compared to the bare membrane. For ESPA2 and EPSA2-PAA, although the latter showed slightly lower water contact angle, smoother surface, and more negative charge, no significant effect on permeate flux and characteristics of the biofilm could be observed by the PAA coating. Moreover, comparing biofouling resistance between the ESPA2-GO and ESPA2-GO-PAA showed that PAA coating slightly reduced the biofouling resistance. These results revealed that, for the membranes tested in this study, the antimicrobial property of the coating is more important than improving physical properties to reduce biofouling. For ESPA2 and ESPA2-PAA, although PAA coating changed the physical properties, *i.e.* hydrophilicity, roughness, and

surface charge, in favor of biofouling resistance, no reduction in biofouling was observed. However, when enhancement in physical properties combined with antimicrobial property by GO coating, better performance was observed for ESPA2-GO compared to ESPA2. The importance of the antimicrobial property of the surface was further highlighted when coating PAA on GO, which slightly decreased biofouling resistance. This might have happened because PAA covered the GO on the surface, making it unavailable to inactivate the bacteria.

Besides the enhancement in biofouling resistance, the well-known antimicrobial property of GO plays a crucial role in removing the biofilm layer from the modified membranes. When bacteria attached to the surface of ESPA2, ESPA2-PD, or ESPA2-PAA, they started to secrete EPS, which helped them to stay firmly attached to the membrane surface and conditioning the membrane surface for further attachment of other foulants [2]. However, GO on the surface of the membranes could inactivate the bacteria, preventing them from sticking to the membrane surface and preventing conditions like EPS secretion for further development of the biofilm [50]. Therefore, the biofilm layer on the GO coated membranes was loosely attached to the surface, resulting in higher flux recovery after washing the membranes with DIW.

4. Conclusion

The surface modification approach was used to reduce the scaling and biofouling on reverse osmosis membranes. GO and PAA were grafted on commercial polyamide RO membranes using a green synthesis method which maintained the permeability of the membranes. ATR-FTIR, Raman, and XPS spectroscopy confirmed coating of the membranes. Analyzing surface properties after coating showed that GO and PAA decreased the membrane surface charge and roughness while increasing the hydrophilicity. These changes in physical properties of the GO-coated membrane as well as the antimicrobial property of GO enhanced the antifouling property of ESPA2-GO performance compared to uncoated ESPA2. On the other hand, PAA coating on the bare membrane only improved scaling resistance with no effect on biofouling, which shows antiscalants can be effective as coating too. PAA coating on GO coated membrane did not improve antiscalant property and had a slightly negative effect on antibiofouling property. Therefore, it was concluded that, for the conditions and membranes tested in this study, enhancement in physical properties are important for scaling resistance;

while for biofouling resistance, antimicrobial property of the surface is crucial. This study presented surface modifications as a potential approach to prevent both scaling and biofouling. Simultaneous presence of the antimicrobial and antiscalining materials (GO-PAA coating) did not have the best antifouling performance, however the effects of the coating on scaling and biofouling was systematically investigated in parallel, and new mechanistic insights on how would surface functional groups/hydrophilicity/charge affect scaling/biofouling were obtained. The findings in this study highlight the importance of the change in the physical and antimicrobial properties of the modified membranes to prevent both scaling and biofouling. To design a nanocomposite coating on RO membranes, a coating with higher hydrophilicity, more negative surface charge, less functional groups to bind with calcium ions, lower roughness, and antimicrobial property would be desirable to increase biofouling and scaling resistance.

Declaration of competing interest

The authors declare that they have no known competing financial interests or personal relationships that could have appeared to influence the work reported in this paper.

Acknowledgment

The authors want to thank Dr. Rich Frank from Hydranautics Inc. for providing the membrane for this research study, Dr. Charisma Lattao for surface ζ -potential measurement, Dr. Mariano Susman for SEM images, Dr. Hoang Nguyen for graphical abstract, and Tayler Hettke for helping with membrane coating. The findings achieved herein are solely the responsibility of the authors.

Appendix A. Supplementary data

Supplementary data to this article can be found online at <https://doi.org/10.1016/j.memsci.2021.119308>.

Funding

This study was funded by NPRP12S-0307-190250 and NPRP13S-0207-200289 from the Qatar National Research Fund, and Welch Foundation award number (E-2011-20190330).

CRediT author statement

Ali Ansari: Investigation of the biofouling work, Formal analysis, Visualization, Writing-Original Draft.

Janire Peña Bahamonde: Investigation of the membrane coating, Formal analysis, Visualization, Writing-Original Draft.

Meng Wang: Investigation of the mineral scaling aspect of the work, Formal analysis, Visualization, Writing-Review and Editing.

Devin L. Shaffer: Writing-Review and Editing.

Yandi Hu: Conceptualization of the mineralization aspect of the work, Methodology, Validation, Supervision, Funding acquisition, Writing-Review and Editing.

Debora F. Rodrigues: Conceptualization of the biofouling and membrane coating aspect of the work, Methodology, Validation, Supervision, Funding acquisition, Writing-Review and Editing.

References

- [1] Z. Yang, D. Saeki, H. Matsuyama, Zwitterionic polymer modification of polyamide reverse-osmosis membranes via surface amination and atom transfer radical polymerization for anti-biofouling, *J. Membr. Sci.* 550 (2018) 332–339.
- [2] Y. Baek, et al., Evaluation of carbon nanotube-polyamide thin-film nanocomposite reverse osmosis membrane: surface properties, performance characteristics and fouling behavior, *J. Ind. Eng. Chem.* 56 (2017) 327–334.
- [3] F. Saffarimandoab, et al., Evaluation of biofouling behavior of zwitterionic silane coated reverse osmosis membranes fouled by marine bacteria, *Prog. Org. Coating* 134 (2019) 303–311.
- [4] H. Alnajjar, et al., Organic fouling control in reverse osmosis (RO) by effective membrane cleaning using saturated CO₂ solution, *Separ. Purif. Technol.* 264 (2021) 118410.
- [5] B. Cao, et al., Gypsum scale formation on graphene oxide modified reverse osmosis membrane, *J. Membr. Sci.* 552 (2018) 132–143.
- [6] A.S. Al-Amoudi, Factors affecting natural organic matter (NOM) and scaling fouling in NF membranes: a review, *Desalination* 259 (1) (2010) 1–10.
- [7] Y. Zarga, et al., Study of calcium carbonate and sulfate co-precipitation, *Chem. Eng. Sci.* 96 (2013) 33–41.
- [8] L.F. Greenlee, et al., The effect of antiscalant addition on calcium carbonate precipitation for a simplified synthetic brackish water reverse osmosis concentrate, *Water Res.* 44 (9) (2010) 2957–2969.
- [9] A. Antony, et al., Scale formation and control in high pressure membrane water treatment systems: a review, *J. Membr. Sci.* 383 (1) (2011) 1–16.
- [10] M. Bystrianský, et al., The presence of ferric iron promotes calcium sulphate scaling in reverse osmosis processes, *Desalination* 393 (2016) 115–119.
- [11] W.-Y. Shih, et al., Ranking of antiscalant performance for gypsum scale suppression in the presence of residual aluminum, *Desalination* 196 (1) (2006) 280–292.
- [12] M.Y. Ashfaq, et al., Isolation, identification and biodiversity of antiscalant degrading seawater bacteria using MALDI-TOF-MS and multivariate analysis, *Sci. Total Environ.* 656 (2019) 910–920.
- [13] J. Peña-Bahamonde, et al., Biological degradation and biostability of nanocomposites based on polysulfone with different concentrations of reduced graphene oxide, *Macromol. Mater. Eng.* 303 (2) (2018) 1700359.
- [14] J. Fan, C.D. Grande, D.F. Rodrigues, Biodegradation of graphene oxide-polymer nanocomposite films in wastewater, *Environ. Sci.: Nano* 4 (9) (2017) 1808–1816.
- [15] Z. Tai, et al., Facile synthesis of Ag/GNS-g-PAA nanohybrids for antimicrobial applications, *Colloids Surf. B Biointerfaces* 89 (2012) 147–151.
- [16] Y. Wang, et al., Improved flux and anti-biofouling performances of reverse osmosis membrane via surface layer-by-layer assembly, *J. Membr. Sci.* 539 (2017) 403–411.
- [17] M.S. Rahaman, et al., Control of biofouling on reverse osmosis polyamide membranes modified with biocidal nanoparticles and antifouling polymer brushes, *J. Mater. Chem. B* 2 (12) (2014) 1724–1732.
- [18] Y. Mansourpanah, E. Momeni Habili, Preparation and modification of thin film PA membranes with improved antifouling property using acrylic acid and UV irradiation, *J. Membr. Sci.* 430 (2013) 158–166.
- [19] J. Peña-Bahamonde, et al., Functionalization of reduced graphene oxide with polysulfone brushes enhance antibacterial properties and reduce human cytotoxicity, *Carbon* 111 (2017) 258–268.
- [20] P.C. Bandara, et al., Investigation of thermal properties of graphene-coated membranes by laser irradiation to remove biofoulants, *Environ. Sci. Technol.* 53 (2) (2019) 903–911.
- [21] H.N. Nguyen, et al., Designing polymeric adhesives for antimicrobial materials: poly(ethylene imine) polymer, graphene, graphene oxide and molybdenum trioxide – a biomimetic approach, *J. Mater. Chem. B* 5 (32) (2017) 6616–6628.
- [22] J.V.D. Perez, et al., Exposure-dependent antimicrobial activity and oxidative properties of polymer-based graphene oxide nanocomposites, *Mater. Sci. Forum* 947 (2019) 13–20.
- [23] P.C. Bandara, et al., Impact of water chemistry, shelf-life, and regeneration in the removal of different chemical and biological contaminants in water by a model Polymeric Graphene Oxide Nanocomposite Membrane Coating, *Journal of Water Process Engineering* 32 (2019) 100967.
- [24] M.Y. Ashfaq, M.A. Al-Ghouti, N. Zouari, Functionalization of reverse osmosis membrane with graphene oxide and polyacrylic acid to control biofouling and mineral scaling, *Sci. Total Environ.* 736 (2020) 139500.
- [25] W.S. Hummers, R.E. Offeman, Preparation of graphitic oxide, *J. Am. Chem. Soc.* 80 (6) (1958), 1339–1339.
- [26] Y. Zhang, S. Zhang, T.-S. Chung, Nanometric graphene oxide framework membranes with enhanced heavy metal removal via nanofiltration, *Environ. Sci. Technol.* 49 (16) (2015) 10235–10242.
- [27] I. Roppolo, et al., A powerful tool for graphene functionalization: benzophenone mediated UV-grafting, *Carbon* 77 (2014) 226–235.
- [28] H. Ma, R.H. Davis, C.N. Bowman, A Novel Sequential Photoinduced Living Graft Polymerization, 2000.
- [29] M. Steenackers, et al., Polymer brushes on graphene, *J. Am. Chem. Soc.* 133 (27) (2011) 10490–10498.
- [30] A. Shaygan Nia, W.H. Binder, Graphene as initiator/catalyst in polymerization chemistry, *Prog. Polym. Sci.* 67 (2017) 48–76.
- [31] Y. Mansourpanah, et al., Enhancing the performance and antifouling properties of nanoporous PES membranes using microwave-assisted grafting of chitosan, *Desalination* 322 (2013) 60–68.
- [32] A. Ansari, et al., Microbially-induced mineral scaling in desalination conditions: mechanisms and effects of commercial antiscalants, *Water Res.* 179 (2020) 115863.
- [33] J. Wang, et al., Improving the water flux and bio-fouling resistance of reverse osmosis (RO) membrane through surface modification by zwitterionic polymer, *J. Membr. Sci.* 493 (2015) 188–199.
- [34] T. Vercellino, et al., The use of covalently attached organo-selenium to inhibit *S. aureus* and *E. coli* biofilms on RO membranes and feed spacers, *Desalination* 317 (2013) 142–151.

- [35] H.N. Nguyen, D.F. Rodrigues, Chronic toxicity of graphene and graphene oxide in sequencing batch bioreactors: a comparative investigation, *J. Hazard Mater.* 343 (2018) 200–207.
- [36] R. Feng, et al., Surface decoration of graphene by grafting polymerization using graphene oxide as the initiator, *J. Mater. Chem.* 22 (9) (2012) 3982–3989.
- [37] H. Ma, R.H. Davis, C.N. Bowman, A novel sequential photoinduced living graft polymerization, *Macromolecules* 33 (2) (2000) 331–335.
- [38] H.M. Hegab, et al., Effective in-situ chemical surface modification of forward osmosis membranes with polydopamine-induced graphene oxide for biofouling mitigation, *Desalination* 385 (2016) 126–137.
- [39] T. Hong Anh Ngo, K. Dinh Do, D. Thi Tran, Surface modification of polyamide TFC membranes via redox-initiated graft polymerization of acrylic acid, *J. Appl. Polym. Sci.* 134 (29) (2017) 45110.
- [40] Y. Zhan, et al., Design of durable and efficient poly(arylene ether nitrile)/bioinspired polydopamine coated graphene oxide nanofibrous composite membrane for anionic dyes separation, *Chem. Eng. J.* 333 (2018) 132–145.
- [41] S. Xia, et al., Preparation of graphene oxide modified polyamide thin film composite membranes with improved hydrophilicity for natural organic matter removal, *Chem. Eng. J.* 280 (2015) 720–727.
- [42] J. Yin, G. Zhu, B. Deng, Graphene oxide (GO) enhanced polyamide (PA) thin-film nanocomposite (TFN) membrane for water purification, *Desalination* 379 (2016) 93–101.
- [43] N.K. Khanzada, et al., Evaluation of anti-bacterial adhesion performance of polydopamine cross-linked graphene oxide RO membrane via in situ optical coherence tomography, *Desalination* 479 (2020) 114339.
- [44] R. Zhang, et al., A novel positively charged composite nanofiltration membrane prepared by bio-inspired adhesion of polydopamine and surface grafting of poly(ethylene imine), *J. Membr. Sci.* 470 (2014) 9–17.
- [45] Q. Cheng, et al., Surface modification of a commercial thin-film composite polyamide reverse osmosis membrane through graft polymerization of N-isopropylacrylamide followed by acrylic acid, *J. Membr. Sci.* 447 (2013) 236–245.
- [46] S. Bano, et al., Graphene oxide modified polyamide nanofiltration membrane with improved flux and antifouling properties, *J. Mater. Chem.* 3 (5) (2015) 2065–2071.
- [47] H. Zhao, et al., Improving the antifouling property of polysulfone ultrafiltration membrane by incorporation of isocyanate-treated graphene oxide, *Phys. Chem. Chem. Phys.* 15 (23) (2013) 9084–9092.
- [48] S.J. Shilton, et al., Raman spectroscopic evaluation of molecular orientation in polysulfone, *Laser Phys. Lett.* 1 (7) (2004) 336–339.
- [49] H.J. Kim, A.E. Fouda, K. Jonasson, In situ study on kinetic behavior during asymmetric membrane formation via phase inversion process using Raman spectroscopy, *J. Appl. Polym. Sci.* 75 (1) (2000) 135–141.
- [50] F. Perreault, M.E. Tousley, M. Elimelech, Thin-film composite polyamide membranes functionalized with biocidal graphene oxide nanosheets, *Environ. Sci. Technol. Lett.* 1 (1) (2014) 71–76.
- [51] K.N. Kudin, et al., Raman spectra of graphite oxide and functionalized graphene sheets, *Nano Lett.* 8 (1) (2008) 36–41.
- [52] Y.M. Lee, et al., Preparation of surface-modified stimuli-responsive polymeric membranes by plasma and ultraviolet grafting methods and their riboflavin permeation, *Polymer* 36 (1) (1995) 81–85.
- [53] G.M. Geise, Why polyamide reverse-osmosis membranes work so well, *Science* 371 (6524) (2021) 31.
- [54] S. Kasemset, et al., Effect of polydopamine deposition conditions on fouling resistance, physical properties, and permeation properties of reverse osmosis membranes in oil/water separation, *J. Membr. Sci.* 425–426 (2013) 208–216.
- [55] J. Wang, et al., Improving the water flux and bio-fouling resistance of reverse osmosis (RO) membrane through surface modification by zwitterionic polymer, *J. Membr. Sci.* 493 (Supplement C) (2015) 188–199.
- [56] H. Jaramillo, et al., Zwitterionic coating on thin-film composite membranes to delay gypsum scaling in reverse osmosis, *J. Membr. Sci.* 618 (2021) 118568.
- [57] M.L. Marré Tirado, et al., Assessing biofouling resistance of a polyamide reverse osmosis membrane surface-modified with a zwitterionic polymer, *J. Membr. Sci.* 520 (2016) 490–498.
- [58] B. Mi, M. Elimelech, Gypsum scaling and cleaning in forward osmosis: measurements and mechanisms, *Environ. Sci. Technol.* 44 (6) (2010) 2022–2028.